JOURNAL OF Materials CHEMISTRY

A solvothermal route to capped nanoparticles of γ-Fe_2O_3 and $CoFe_2O_4$

Srinivasa Thimmaiah,[a] Michael Rajamathi,[b] Nikhil Singh,[a]† Parthasarathi Bera,[a] Fiona Meldrum,[c] N. Chandrasekhar[d]‡ and Ram Seshadri[a]

[a]*Solid State and Structural Chemistry Unit, Indian Institute of Science, Bangalore 560 012, India. Fax: (91) 80 360 1310; E-mail: seshadri@sscu.iisc.ernet.in*
[b]*Department of Chemistry, St. Joseph's College, Bangalore 560 025, India*
[c]*Department of Chemistry, Queen Mary, University of London, Mile End Road, London, UK E1 4NS. E-mail: f.c.meldrum@qmul.ac.uk*
[d]*School of Physics and Astronomy, University of Minnesota, 116 Church St. SE, Minneapolis, MN 55455, USA. E-mail: nchandra@physics.umn.edu*

Received 9th May 2001, Accepted 14th August 2001
First published as an Advance Article on the web 18th October 2001

The decomposition of single or multiple transition metal cupferron complexes in organic solvents under solvothermal conditions and in the presence of long chain amines yields the corresponding oxide nanoparticles. The examples presented here are maghemite γ-Fe_2O_3 nanoparticles from an Fe^{III}–cupferron complex and spinel $CoFe_2O_4$ nanoparticles starting from Co^{II}–cupferron complex and Fe^{III}–cupferron complex taken in suitable proportions. The nanoparticles are capped with *n*-octylamine or *n*-dodecylamine. The presence of amine in the reaction is found to be essential for the formation of the product. The magnetic behavior of pressed pellets of these nanoparticles is presented.

Introduction

There is great interest in the preparation of transition metal oxide nanoparticles as a result of their finding extensive use in high-performance ceramics,[1] as media for magnetic data storage,[2] in catalysis,[3] for solar energy conversion,[4] and in the preparation of ferrofluids.[5] Despite these applications, methods for the preparation of monodisperse oxide nanoparticles in the sub-10 nm size regime have by no means attained the synthetic sophistication that is routine in the preparation of noble metal[6] or II–VI semiconductor chalcogenide nanoparticles.[7] For example, the reduction of metals such as gold in organic solvents in the presence of capping agents affords highly monodisperse, crystalline nanoparticles whose size can be carefully controlled.[6,8] Likewise, the reaction of organocadmium precursors with a chalcogen source in a solvent that doubles as a capping agent yields crystalline semiconducting chalcogenide nanoparticles whose band gaps can be controlled through control of size.[7,9]

Transition metal oxides do not easily lend themselves to such routes of preparation. The direct oxidation of metals is usually exothermic resulting in sintering. Also, it is difficult to envisage oxygen sources (as opposed to chalcogen sources) in solution. As a result, transition metal oxides are usually prepared by so-called hydrolytic routes wherein the solvation sheets of water around a metal ion are dehydrated under alkaline conditions. Assuming six water molecules in its solvation shell, the complete dehydration of a trivalent ion to the corresponding oxide could be written:

$$2M^{3+}(H_2O)_6 \rightarrow M_2O_3\downarrow + 6H^+ + 9H_2O$$

Such a scheme illustrates the necessity for alkaline conditions. Unfortunately, most metal ions have high solvation energies and schemes such as this one often become valid only at temperatures where formation of oxide is accompanied by sintering. While for certain materials (notably Fe^{III} oxides such as $CoFe_2O_4$) hydrolytic routes remain useful, there are a number of metals whose nanoparticulate oxides require alternate routes of preparation. Early transition metals such as Ti and Zr form alkoxides that can be carefully decomposed to the corresponding oxide nanoparticles. Chemseddine and Moritz[10] have used this strategy to make monodisperse TiO_2 (anatase) nanoparticles in a variety of sizes with different crystal habits. Colvin and coworkers[11] have followed earlier work[12] in using the metathetic reaction between titanium alkoxides and titanium halides (with elimination of the corresponding alkyl halide) to prepare soluble, capped (with trioctylphosphine oxide, TOPO) anatase nanoparticles.

Rockenberger, Scher and Alivisatos[13] have described what is so far perhaps the most general route for the preparation of oxide nanoparticles. Their route involves the decomposition of cupferron (*N*-nitroso-*N*-phenylhydroxylamine) complexes of metal ions such as Fe^{3+}, Cu^{2+} and Mn^{3+} in the high temperature solvent trioctylamine at temperatures around 300 °C or lower obtaining the respective oxides γ-Fe_2O_3, Mn_3O_4 and Cu_2O. In this non-hydrolytic route, the cupferron complex (which binds to the metal ion through oxygen) is decomposed releasing a leaving group such as nitrosobenzene. These decompositions take place at sufficiently low temperatures (between 150 and 300 °C for most metals) that (i) the reactions can be performed in solvents and (ii) a capping agent such as a long chain amine can be employed to prevent sintering and to prepare *soluble* nanoparticles. The importance of being able to prepare soluble nanoparticles cannot be overemphasized. Solubilization is the most important step in being able to perform size selective precipitations (using solvent/non-solvent pairs)[7,14] and in being able to assemble

†Permanent Address: Department of Ceramic Engineering, Institute of Technology, Benares Hindu University, Varanasi 221 005 India.
‡Permanent Address: Physics Department, Indian Institute of Science, Bangalore 560 012 India. E-mail: chandra@physics.iisc.ernet.in

superlattices of the nanoparticles.[15,16] Already, the self-assembly of magnetic superlattices has received some attention.[17]

In this publication, we attempt to extend the work of Alivisatos and coworkers in the following way: (i) we show that relatively expensive (and toxic) amines can be replaced as solvents by using toluene albeit under solvothermal conditions; (ii) mixed transition metal oxides such as the spinel $CoFe_2O_4$ can also be prepared using the cupferron complex route, by using two precursors instead of one. Pressed pellets of the nanoparticles are superparamagnetic at room temperature.

Acicular γ-Fe_2O_3 nanoparticles for magnetic data storage are typically prepared by the hydrolysis of Fe^{II} salts to goethite, dehydration to haematite, reduction to magnetite and finally re-oxidation to maghemite.[18] A number of recent papers have focussed on the preparation of sub-10 nm γ-Fe_2O_3 nanoparticles in polymer matrices,[19] through hydrolysis follwed by size-selection,[20] and by hydrolysis of iron (II)-based surfactants.[21] Morales and coworkers[22] have recently described in great detail the magnetism of γ-Fe_2O_3 nanoparticles of various sizes.

Interest in the preparation of spinel $CoFe_2O_4$ nanoparticles stems from their potential as magnetic media for data storage. Bulk $CoFe_2O_4$ displays strong magnetic anisotropy as well as large saturation magnetization and coercivity. Haneda and Morrish[23] have investigated the magnetic structure of $CoFe_2O_4$ nanoparticles as a function of particle size. The $CoFe_2O_4$ particles used in magnetic fluids have been shown as displaying multiaxial anisotropy.[24] Recent reports on $CoFe_2O_4$ nanoparticles include their synthesis in reverse micelle microemulsions,[25] using Co- and Fe-containing surfactants as the metal sources[26] and using sonochemistry to accelerate the decomposition of carbonyl precursors.[27] Ammar *et al.*[28] have recently reported the preparation of $CoFe_2O_4$ nanoparticles by hydrolysis of the metal salts in propylene glycol. The magnetic properties of their nanoparticles have been subject to extensive study.

Experimental

The Fe(III) cupferron complex $Fe(cupf)_3$ was prepared following standard procedures by dissolving 6.5 g of AR grade ferric alum, $(NH_4)Fe(SO_4)_2{\cdot}12H_2O$, in 150 cm^3 of water. To this solution, 125 cm^3 of conc. HCl was added and the mixture was cooled to 0 °C. A 5% by weight filtered cupferron (*N*-nitroso-*N*-phenylhydroxylamine, ammonium salt) solution (also cooled to 0 °C) was then added with vigorous stirring. The brown precipitate was collected, washed with dil. HCl and then with 5 M ammonia solution to remove excess cupferron. The complex was then recrystallized from heptane, and characterized by thermogravimetry and infrared spectroscopy. The preparation of the Co(II) cupferron complex $Co(cupf)_2$ was carried out in neutral conditions by chilling a solution of 5 g of $CoCl_2{\cdot}6H_2O$ in 100 cm^3 of water to 0 °C and then adding a chilled 5% by weight filtered cupferron solution in water. The deep pink precipitate was recrystallized from methanol, and characterized by thermogravimetry and infrared spectroscopy. Fig. 1 displays the results of the thermogravimetric analysis of the precursor cupferron complexes under an inert (nitrogen) atmosphere.

In a typical experiment, iron oxide nanoparticles were prepared by taking 0.75 g (1.45 mmol) of the $Fe(cupf)_3$ complex, 2 cm^3 of *n*-octylamine (or *n*-dodecylamine) and 48 cm^3 of toluene in a Teflon-gasketted SS316 bomb (corresponding to 70% filling of the bomb). The sealed bomb was placed for 1 h in a hot-air oven that had been preheated to 220 °C, after which it was quenched to room temperature by removal from the oven. A viscous deep-brown solution with suspended particles formed. Most of the solid product could be recovered by precipitating the solution through addition of 2-propanol, which serves to increase the solvent polarity. Washing of the product (assisted by its magnetism) was carried out with 2-propanol until the infrared spectra did not display any trace of the original cupferron complex.

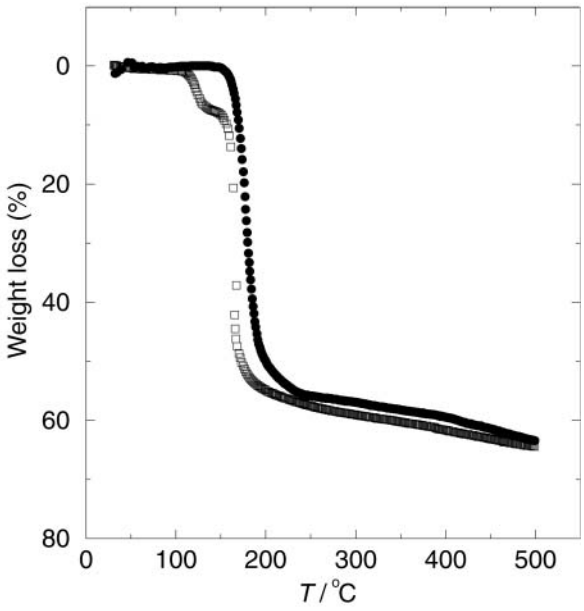

Fig. 1 Weight loss under a nitrogen atmosphere as a function of temperature for the $Fe(cupf)_3$ precursor (circles) and for the $Co(cupf)_2$ precursor (squares).

Cobalt ferrite nanoparticles were prepared in a similar manner by taking an initial charge containing 0.30 g (0.80 mmol) of $Co(cupf)_2$ and 0.83 g (1.6 mmol) of $Fe(cupf)_3$ and fixing amounts of amine and toluene as described previously. By itself, $Co(cupf)_2$ does not decompose into an X-ray crystalline oxide, but instead, $Co(OH)_2$ is formed.

Powder XRD patterns were acquired in the θ–2θ Bragg–Brentano geometry on a Siemens D5005 diffractometer using CuKα radiation with a scan rate of 1° 2θ per minute. The data were rebinned into 0.06 or 0.10° steps in order to improve statistics.

Samples were prepared for TEM by placing a drop of the toluene suspension of the nanoparticles on carbon-coated, Formvar-covered Cu TEM grids and subsequently drawing off excess solvent. The grids were examined using a JEOL 2000EX TEM operating at 120 kV.

EDX analysis of the cobalt ferrite nanoparticles made use of a Link ISIS system attached to a JEOL JSM 5600LV scanning electron microscope. Core level X-ray photoelectron spectra of the cobalt ferrite nanoparticles were recorded using AlKα incident X-rays on a Vaccuum Generators ESCA 3 Mk II instrument.

Pressed pellets of the samples were subject to magnetic measurement using a Quantum Design SQUID magnetometer.

Results and discussion

Preparation

Solving for the three volume roots in the Peng–Robinson equation of state[29] as a function of different pressures and temperatures, and using as inputs the density of solvent in the bomb and tabulated acentric factors and critical constants for toluene, allows one to plot isobars of the molar volume of solvent in the bomb as a function of temperature. This permits us to estimate upper bounds for the pressure within the bomb and we find that this is always less than 100 bar for the temperatures and filling fractions used in the present system.

We find that the amine plays an important rôle in the

formation of oxide nanoparticles in the present systems, apart from capping the nanoparticles after they are formed. When no amine is used during the decomposition of $Fe(cupf)_3$, a reddish-brown non-magnetic product is formed (perhaps an oxide–hydroxide) that is nearly X-ray amorphous. For the amounts of the $Fe(cupf)_3$ complex and toluene that were taken, it was found that less than 1 cm^3 of the amine did not result in any magnetic product. In order to verify whether the amine contributed solely by increasing the reaction pH, we attempted the decomposition of the $Fe(cupf)_3$ under solvothermal conditions in the presence of triethylamine. This did not yield any magnetic particles either.

As mentioned in the introduction, an important issue in the preparation of the nanoparticles is their ability to dissolve/disperse in suitable solvents. Since long-chain amines are being used in the present case to cap the nanoparticles, we expected the product nanoparticles to be soluble in non-polar solvents such as toluene. Indeed, as prepared, suspended particles can be removed from the brown solution magnetically to give clear brown solutions from which magnetic powders can be further precipitated through the addition of a polar solvent such as 2-propanol. This suggests that the as-prepared nanoparticles are soluble in toluene. Unfortunately, once the solid material is collected and dried, it displays great reluctance to go back into toluene solution. Alivisatos and coworkers[13] similarly report their air-dried nanoparticles as being difficult to redisperse in organic solvents.

Characterization

Fig. 2 displays experimental and fitted powder X-ray diffraction profiles of *n*-octylamine-capped nanoparticles of (a) γ-Fe_2O_3 and (b) $CoFe_2O_4$. The data were treated using the Rietveld method[30] using as models the tetragonal defect spinel crystal structure of γ-Fe_2O_3[31] and the cubic spinel structure of $CoFe_2O_4$.[32] Scale factors, lattice and profile parameters were freed for the refinement. The high background of the profiles arises due to fluorescence from the Fe and Co atoms. The Rietveld fits support the assignments of the crystal structures, as do the expected peak positions which are displayed as vertical lines. The refined cell parameters for γ-Fe_2O_3 were $a=b=8.38(9)$ Å and $c=8.4(2)$ Å, while for $CoFe_2O_4$ it was $a=8.38(2)$ Å. Co and Fe have very similar X-ray scattering lengths so it is difficult from diffraction data such as those shown to assign site selection in the spinel structure. In order to establish the formation of $CoFe_2O_4$, we have additionally carried out an EDX analysis which consistently yielded a Co : Fe atom ratio of 1 : 2 within a 6% error.

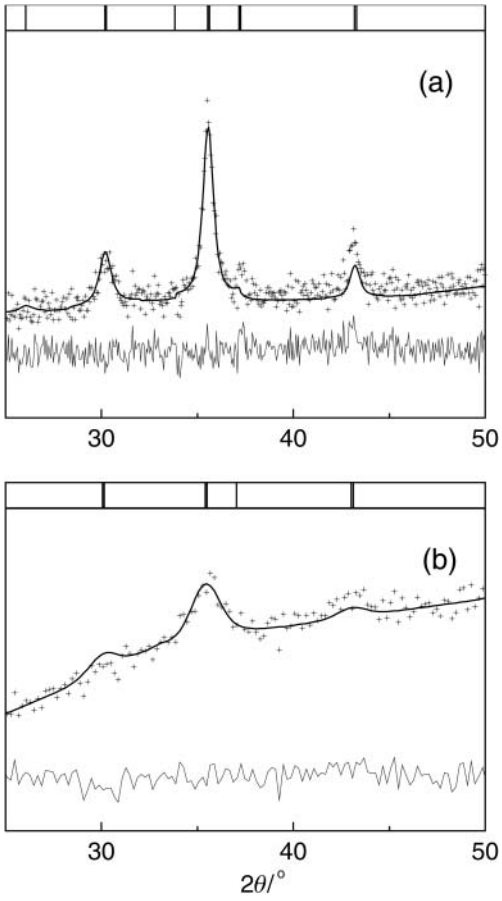

Fig. 2 Rietveld refined powder X-ray diffraction patterns of (a) the *n*-octylamine-capped γ-Fe_2O_3 nanoparticles and of (b) the *n*-octylamine-capped $CoFe_2O_4$ nanoparticles. The vertical lines at the tops of the two panels are expected peak positions.

We have attempted to establish the oxidation states of Co and Fe in the $CoFe_2O_4$ nanoparticles using core-level X-ray photoelectron spectroscopy. Co 2p and Fe 2p core level spectra of a pellet of nanoparticles are displayed in Fig. 3. The raw data could be decomposed into four contributions corresponding to $2p_{3/2}$ and $2p_{1/2}$ and each with its satellite. The positions of the peaks in the spectra were adjusted for sample charging by using the C 1s signal at 285 eV as a reference. From this we obtained a 2p binding energy for Co of 781.9 eV, and for Fe the 2p binding energy was 712.3 eV. These values are in the range of what are expected for oxidic Co^{II} and Fe^{III} respectively.[33] We note that these oxidation states are also consistent with the fact that individually and under the present conditions, the cupferron complexes decompose to give Co^{II} and Fe^{III} species. By integrating the core-level intensities, it was possible to obtain, through the use of standard formulae,[33] an Fe : Co ratio of 1.8 which is close to the ratio obtained by EDX analysis.

Transmission electron microscopy images of *n*-octylamine-capped γ-Fe_2O_3 and $CoFe_2O_4$ nanoparticles along with histograms of the particle diameters (as insets) are presented in Fig. 4 and Fig. 5. The particles are seen to be nearly

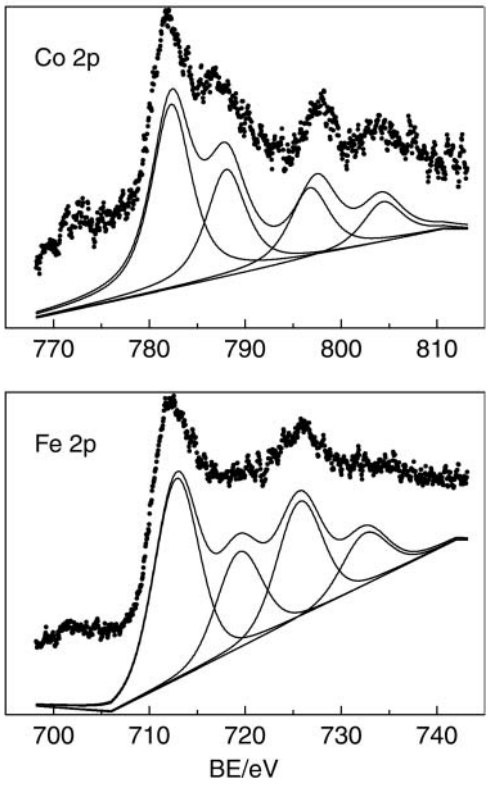

Fig. 3 Core level XP spectra in the Co and Fe 2p core photoelectron regions. The decomposition of the spectra is described in the text.

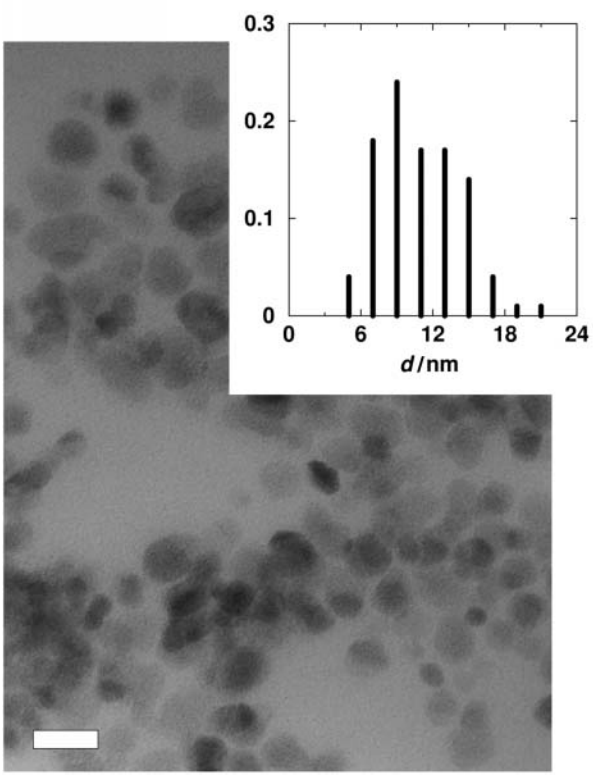

Fig. 4 Transmission electron micrograph of the *n*-octylamine-capped γ-Fe_2O_3 nanoparticles. The inset is a histogram of the diameters. The bar is 20 nm.

spheroidal. The γ-Fe_2O_3 nanoparticles possess a mean diameter of 10.4 nm with a standard deviation of 3.5 nm. The $CoFe_2O_4$ nanoparticles on the other hand are significantly smaller, with a mean diameter of 7.3 nm with a standard deviation of 1.5 nm. The ratios of the standard deviation to the mean are respectively 34% and 20% for the nanoparticles in Fig. 4 and Fig. 5. Since the preparative conditions in terms of temperature and concentrations are nearly identical, it is interesting to understand why one obtains smaller, more monodisperse nanoparticles in the case of $CoFe_2O_4$. We believe the reason to be that $Co(cupf)_2$ decomposes at a temperature of 165 °C (the midpoint in the thermogravimetric trace) which is significantly lower than the 180 °C at which $Fe(cupf)_3$ decomposes (see Fig. 1). Therefore, while in the preparation of $CoFe_2O_4$ at 220 °C, a number of nuclei are rapidly formed that are then permitted to grow, fewer nuclei form in the γ-Fe_2O_3 preparation experiment, which means that particles can grow larger, and nucleation and growth are less well separated. The separation of nucleation and growth is an important condition for the preparation of monodisperse nanoparticles.[34]

We have attempted to use a longer chain amine—*n*-dodecylamine instead of *n*-octylamine—in the hope that a longer, more hydrophobic chain might prevent particle growth and yield smaller particles. This assumption seems to be correct in the case of γ-Fe_2O_3 nanoparticles prepared with *n*-dodecylamine capping (all other conditions being kept the same). The micrograph in Fig. 6 shows that *n*-dodecylamine-capped γ-Fe_2O_3 nanoparticles have a diameter distribution that peaks at 7.2 nm with a standard deviation of 1.3 nm which is 18% of the mean. This means that the as-prepared nanoparticles have a monodispersity that is close to what is needed in order to construct superlattices—when the standard deviation in the particle size distribution is less than about 10%, nanoparticle aggregates start displaying short-range order and when the monodispersity is even smaller, crystalline superlattice self-assembly is known to take place.

The capping of the nanoparticles was established by using thermogravimetry in air, and infrared spectroscopy. Fig. 7 displays the sample weight loss as a function of temperature (at a heating rate of 10 °C min^{-1}) for the *n*-octylamine-capped γ-Fe_2O_3 nanoparticles (circles) and $CoFe_2O_4$ nanoparticles (squares). The samples show, respectively, weight losses of

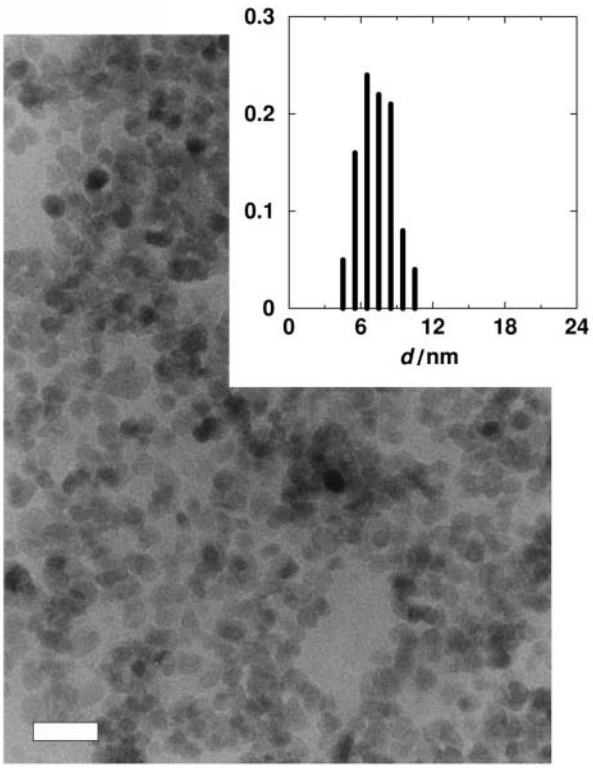

Fig. 5 Transmission electron micrograph of the *n*-octylamine-capped $CoFe_2O_4$ nanoparticles. The inset is a histogram of the diameters. The bar is 20 nm.

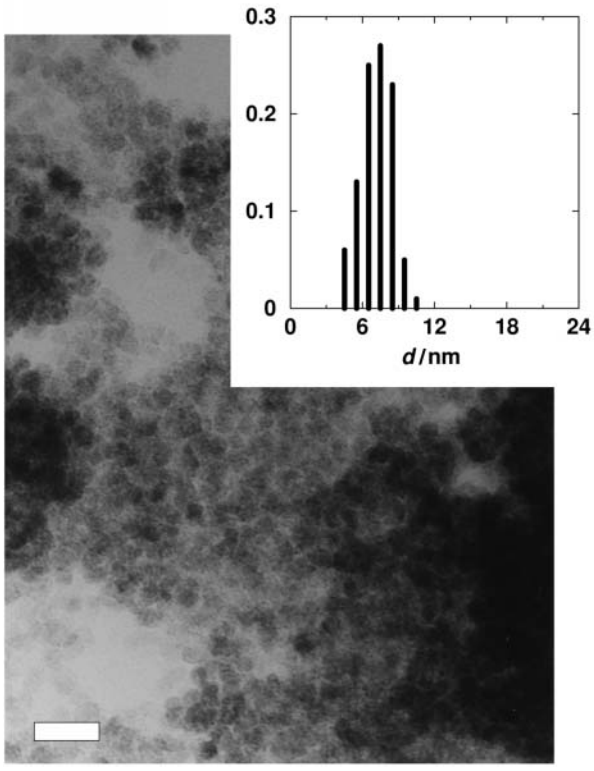

Fig. 6 Transmission electron micrograph of the *n*-dodecylamine-capped γ-Fe_2O_3 nanoparticles. The inset is a histogram of the diameters. The bar is 20 nm.

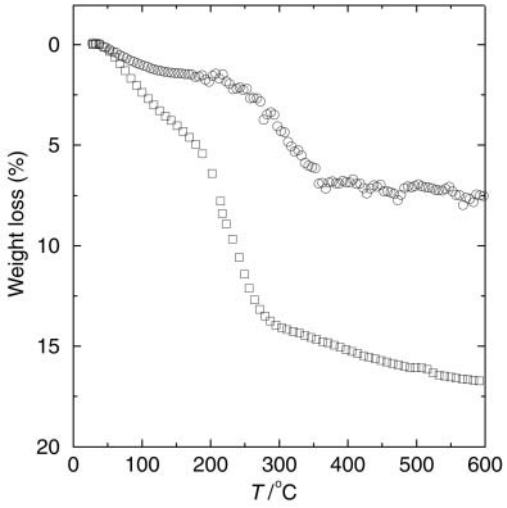

Fig. 7 Weight loss in air as a function of temperature for the *n*-octylamine-capped γ-Fe_2O_3 nanoparticles (circles) and for the *n*-octylamine-capped $CoFe_2O_4$ nanoparticles (squares).

7.5% and 16.5%, with the weight losses being nearly complete by about 400 °C. We ascribe this weight loss to the air oxidation of the total organic matter on the nanoparticle surface. The γ-Fe_2O_3 nanoparticles are found to convert to crystalline α-Fe_2O_3 as verified by powder XRD, while the $CoFe_2O_4$ samples are seen to retain the spinel structure but they become more crystalline. If we assume the weight loss is due to capping *n*-octylamine molecules and use the average dimensions obtained from the TEM images, we can estimate the number density of capping molecules on the nanoparticle surface by assuming the nanoparticles possess bulk density. For the 10 nm γ-Fe_2O_3 nanoparticles, we obtain an estimate of 1 amine molecule cap for every 33 $Å^2$ of nanoparticle surface. For the 7.3 nm $CoFe_2O_4$ particles, the 16.5% weight loss corresponds to a capping density of 1 amine molecule for every 17 $Å^2$ of nanoparticle surface. In obtaining these estimates, a number of assumptions are made. Nevertheless, they suggest that there is a nearly close-packed monolayer of *n*-octylamine molecules that cap the nanoparticles and prevent their aggregation.

FTIR spectra of the nanoparticles, focusing on the region of the C–H stretch, are displayed in Fig. 8. The peaks are identified as arising from the symmetric and asymmetric methylene and $–CH_3$ vibrations. The peak positions are in the following wavenumber ranges: $–CH_2–$ sym at 2852, $–CH_2–$ asym at 2922, $–CH_3$ sym at 2872 and $–CH_3$ asym at 2956 cm^{-1}. The wavenumbers are in the range expected of all-*trans* chains—for *gauche* chains, the peak positions would be slightly shifted to higher wavenumber.[35] If the chains are all-*trans*, this means that they are relatively rod-like and one can infer that the capping molecules stick out radially from the spherical nanoparticle surface.

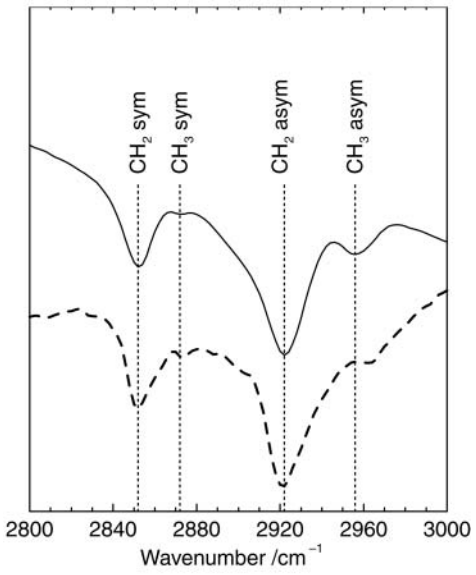

Fig. 8 FTIR spectra of the nanoparticles showing the region of the C–H stretch. The solid line is for γ-Fe_2O_3 and the dashed line for $CoFe_2O_4$.

Magnetic properties

Fig. 9 displays, in its various panels, the magnetization of the *n*-octylamine-capped γ-Fe_2O_3 nanoparticles. The 200 Oe magnetization as a function of temperature shown in panel (a) suggests that while the nanoparticles are indeed ferrimagnetic, the field-cooled (FC) and zero-field cooled (ZFC) data are already separated at 300 K. These nanoparticles have a mean diameter of 10.4 nm, which is at the border between superparamagnetism and ferrimagnetism. The separation of these traces perhaps arises due to the larger particles in the pellet. *M versus H* magnetization loops shown in panel (b) for data acquired at 300, 250 and 200 K, and in panel (c) for data acquired at 150, 100 and 50 K suggest that for the most part, the sample is superparamagnetic and that the superparamagnetism is "blocked" between 150 K and 200 K. Plots of *M versus H*/*T* should collapse on to a single hysteresis-free trace for a superparamagnetic sample. This is indeed seen in panel (d) for data acquired at 300, 250 and 200 K. At the lower temperatures of 150, 100 and 50 K [panel (e)] this coalescense is no longer seen suggesting that the superparamagnetism is indeed blocked. At no temperature is there a well-defined hysteresis. The saturation magnetization of about 56 emu g^{-1}

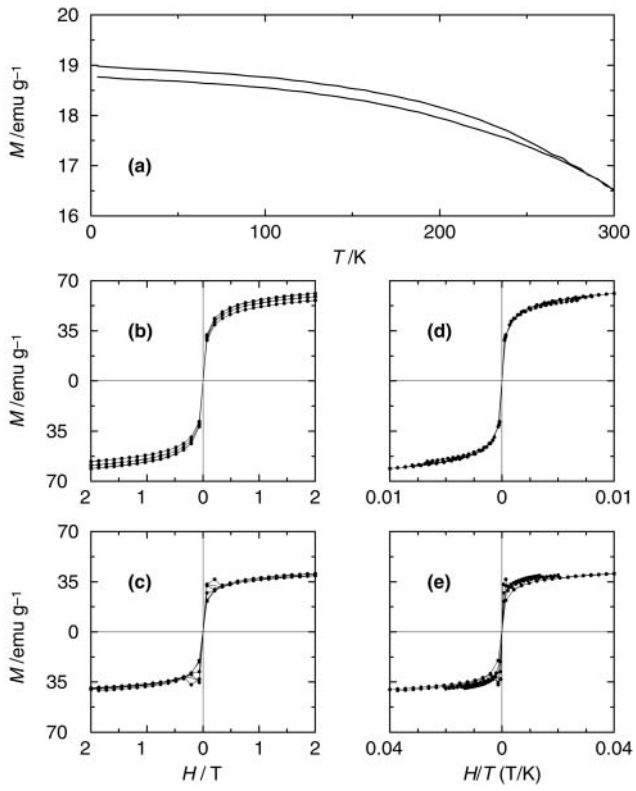

Fig. 9 (a) Magnetization as a function of temperature under a 200 Oe field of a pressed pellet of the *n*-octylamine-capped γ-Fe_2O_3 nanoparticles. The lower trace corresponds to zero-field cooling (ZFC) and the upper trace to field cooling (FC). (b) Magnetization loops of the nanoparticles at 300, 250, 200 K. (c) Magnetization loops at 150, 100 and 50 K. (d) *M vs. H*/*T* at 300, 250, 200 K. (e) *M vs. H*/*T* at 150, 100 and 50 K.

correlates well with the titration presented by Morales *et al.*[22] of saturation magnetization as a function of particle size for γ-Fe_2O_3 nanoparticles, though these authors do warn that magnetic properties of iron oxide nanoparticles are strongly influenced by the preparative procedure.

Fig. 10 similarly displays the magnetic properties as a function of temperature for the $CoFe_2O_4$ nanoparticles. We recollect that these nanoparticles are smaller (mean diameter of 7.3 nm) and a little more monodisperse. $CoFe_2O_4$ is the harder magnet however, so larger coercivities can be expected. The *M versus T* plots obtained at fields of 200 Oe (solid line) and 1000 Oe (dashed line) show a ZFC–FC separation between 100 and 150 K though the precise temperature of the splitting is different at the different fields. *M versus H* plots are displayed for data taken at 300, 250, 200 and 150 K in panel (b) and at 100 K and 50 K in panel (c). The *M versus H* plots show that hysteresis develops below 100 K, and the coercive field of this sample is 430 Oe at 100 K and 3000 Oe at 50 K. Corresponding to the *M versus H* plots, the plots of *M versus H*/*T* coalesce above 100 K [panel (d)], while at 100 K and 50 K [panel (e)] they are separated. In the case of the $CoFe_2O_4$ nanoparticles, the separation of FC and ZFC is thus seen to trace the magnetization behavior.

Conclusion

We have demonstrated that solvothermal conditions involving inexpensive solvents can be employed to prepare capped oxide nanoparticles of transition metal oxides through the decomposition of suitable precursors. The oxides prepared by this method in nanoparticulate form—γ-Fe_2O_3 and $CoFe_2O_4$—are only representative of a number of single or mixed transition metal oxides that are amenable to such a preparative strategy.

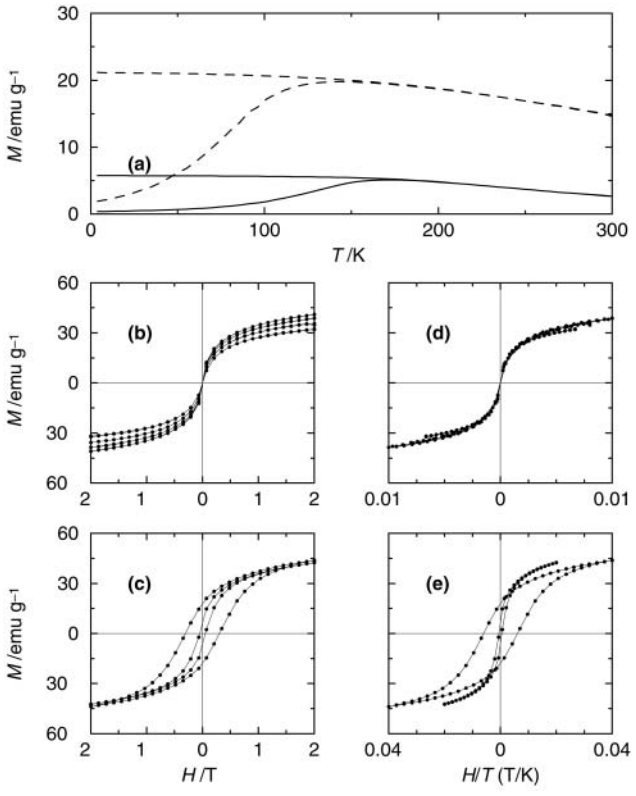

Fig. 10 (a) Magnetization as a function of temperature under a 200 Oe field (solid line) and under a 1000 Oe field (dashed line) of a pressed pellet of the *n*-octylamine-capped $CoFe_2O_4$ nanoparticles. The lower traces correspond to ZFC and the upper traces to FC. (b) Magnetization loops of the nanoparticles at 300, 250, 200, and 150 K. (c) Magnetization loops at 100 and 50 K. (d) *M vs. H*/*T* at 300, 250, 200 and 150 K. (e) *M vs. H*/*T* at 100 and 50 K.

The magnetic behavior of the nanoparticles so prepared are in keeping with what is expected for materials in these size regimes. The important challenge of finding suitable conditions for the redissolution of these oxide nanoparticles and the corollary of being able to perform size-selective precipitation is yet to be tackled. We expect that this might be a simple matter of finding the right combination of particle size, capping agent and solvent system.

Acknowledgements

We are grateful to Professor A. M. Goldman and Dr. Anand Bhattacharya for use of and help with the magnetometer, and Professor M. S. Hegde for use of the XP spectrometer. We thank Professor S. Vasudevan and Dr. M. Giridhar for helpful suggestions. This work has been supported by the Department of Science and Technology, India.

References

1 R. A. Andrievski, *J. Mater. Sci.*, 1994, **29**, 614.
2 S. Onodera, H. Kondo and T. Kawana, *MRS Bull.*, 1996, **21**, 35.
3 J. A. Schwarz, C. Contescu and A. Contescu, *Chem. Rev*, 1995, **95**, 477.
4 A. Hagfeldt and M. Grätzel, *Chem. Rev*, 1995, **95**, 49.
5 V. Cabuil, *Curr. Opin. Colloid Interface Sci.*, 2000, **5**, 44.
6 M. Brust, M. Walker, D. Bethell, D. J. Schiffrin and R. Whymann, *J. Chem. Soc., Chem. Commun.*, 1994, 801.
7 C. B. Murray, D. J. Norris and M. G. Bawendi, *J. Am. Chem. Soc.*, 1993, **115**, 8706.
8 R. L. Whetten, J. T. Khoury, M. M. Alvarez, S. Murthy, I. Vezmar, Z. L. Wang, P. W. Stephens, C. L. Cleveland, D. W. Luedtke and U. Landmann, *Adv. Mater.*, 1996, **8**, 428.
9 M. Nirmal and L. Brus, *Acc. Chem. Res.*, 1999, **32**, 407.
10 A. Chemseddine and T. Moritz, *Eur. J. Inorg. Chem.*, 1999, 235.
11 T. J. Trentler, T. E. Denler, J. F. Bertone, A. Agrawal and V. L. Colvin, *J. Am. Chem. Soc.*, 1999, **121**, 1613.
12 P. Arnal, R. J. P. Corriu, D. Leclerq, P. H. Mutin and A. Vioux, *Chem. Mater.*, 1997, **9**, 694.
13 J. Rockenberger, E. C. Scher and A. P. Alivisatos, *J. Am. Chem. Soc.*, 1999, **121**, 11595.
14 A. Chemseddine and H. Weller, *Ber. Bunsen-Ges. Phys. Chem.*, 1993, **97**, 636.
15 C. A. Murray and D. G. Grier, *Annu. Rev. Phys. Chem.*, 1996, **47**, 421.
16 C. P. Collier, T. Vossmeyer and J. R. Heath, *Annu. Rev. Phys. Chem.*, 1998, **49**, 371.
17 S. Sun, C. B. Murray, D. Weller, L. Folks and A. Moser, *Science*, 2000, **287**, 1989; C. T. Black, C. B. Murray, R. L. Sandstrom and S. Sun, *Science*, 2000, **290**, 1131.
18 A. Tasaki, K. Tagawa, E. Kita, S. Harada and T. Kusunose, *IEEE Trans. Magn.*, 1981, **17**, 3026.
19 R. F. Ziolo, E. P. Giannelis, B. A. Weinstein, M. P. O'Horo, B. N. Ganguly, V. Mehrotra, M. W. Russel and D. R. Huffman, *Science*, 1992, **257**, 219.
20 S. Lefebure, E. Dubois, V. Cabuil, S. Neveu and R. Massart, *J. Mater. Res.*, 1998, **13**, 2975.
21 N. Feltin and M. P. Pileni, *Langmuir*, 1997, **13**, 3927.
22 M. P. Morales, S. Veintemillas-Verdaguer, M. I. Montero, C. J. Serna, A. Roig, Ll. Casas, B. Martínez and F. Sandiumenge, *Chem. Mater.*, 1999, **11**, 3058.
23 K. Haneda and A. H. Morrish, *J. Appl. Phys.*, 1988, **63**, 4258.
24 K. J. Davies, S. Wells, R. V. Upadhyay, S. W. Charles, K. O'Grady, M. E. Hilo, T. Meaz and S. Mørup, *J. Magn. Magn. Mater.*, 1995, **149**, 14.
25 V. Pillai and D. O. Shah, *J. Magn. Magn. Mater.*, 1996, **163**, 243.
26 N. Moumen, P. Veillet and M. P. Pileni, *J. Magn. Magn. Mater.*, 1995, **149**, 67.
27 K. V. P. M. Shafi, A. Gedanken, R. Prozorov and J. Balogh, *Chem. Mater.*, 1998, **10**, 3445.
28 S. Ammar, A. Helfen, N. Jouini, F. Fiévet, I. Rosenman, F. Villain, P. Molinié and M. Danot, *J. Mater. Chem.*, 2001, **11**, 186.
29 R. C. Reed, J. M. Prausnitz and B. E. Poling, *The Properties of Liquids and Gases*, 4th edn., McGraw-Hill Book Company.
30 Rietveld refinements made use of version 1.20 of the XND Rietveld code: J.-F. Bérar and P. Garnier, *NIST Spec. Publ.*, 1992, **846**, 212.

31 C. Greaves, *J. Solid State Chem.*, 1983, **49**, 325.
32 T. Inoue, *J. Electrochem. Soc. Jpn.*, 1955, **23**, 24.
33 D. Briggs and M. P. Seah, *Practical Surface Analysis by Auger and X-ray Photoelectron Spectroscopy*, 2nd edn., John Wiley and Sons, New York, 1990.
34 V. K. LaMer and R. H. Dinegar, *J. Am. Chem. Soc.*, 1950, **72**, 4847.
35 R. A. MacPhail, H. L. Strauss, R. G. Snyder and C. A. Elliger, *J. Phys. Chem.*, 1984, **88**, 334; R. G. Snyder, H. L. Strauss and C. A. Elliger, *J. Phys. Chem.*, 1982, **86**, 5145.